J. Fluid Mech. (1994), *vol.* 264, *pp.* 303–319

Solitary waves on a vorticity layer

By F. J. HIGUERA AND J. JIMÉNEZ
E.T.S. Ingenieros Aeronáuticos, Pza. Cardenal Cisneros 3, 28040 Madrid, Spain

(Received 21 January 1993 and in revised form 9 September 1993)

Contour dynamics methods are used to determine the shapes and speeds of planar, steadily propagating, solitary waves on a two-dimensional layer of uniform vorticity adjacent to a free-slip plane wall in an, otherwise irrotational, unbounded incompressible fluid, as well as of axisymmetric solitary waves propagating on a tube of azimuthal vorticity proportional to the distance to the symmetry axis. A continuous family of solutions of the Euler equations is found in each case. In the planar case they range from small-amplitude solitons of the Benjamin–Ono equation to large-amplitude waves that tend to one member of the touching pair of counter-rotating vortices of Pierrehumbert (1980), but this convergence is slow in two small regions near the tips of the waves, for which an asymptotic analysis is presented. In the axisymmetric case, the small-amplitude waves obey a Korteweg–de Vries equation with small logarithmic corrections, and the large-amplitude waves tend to Hill's spherical vortex.

1. Introduction

In this paper we describe permanent solitary waves propagating on a two-dimensional layer of uniform vorticity attached to a wall. These waves were first described in Jiménez & Orlandi (1993), where a vorticity layer of finite length was used to model the generation of concentrated streamwise vortices in a turbulent channel. It had been observed that layers of concentrated streamwise vorticity form near the wall in turbulent channels, and that they later roll into streamwise vortices (Sendstad 1992). Jiménez & Orlandi (1993) was an attempt to model this process by studying the behaviour of a two-dimensional inviscid vorticity layer near a wall. It was argued that this model should approximate the behaviour of a turbulent channel in planes perpendicular to the mean flow velocity.

It was found, by direct numerical integration of the initial value problem, that the layer disintegrates into discrete vortices which later propagate along the wall without apparent change of shape. Because of the effect of the image vorticity reflected by the wall, these isolated vortices are equivalent to vortex dipoles, and correspond to the touching vortex dipoles obtained by Pierrehumbert (1980). Jiménez & Orlandi also derived an integro-differential equation to model the behaviour of the layer for perturbations of long wavelength, whose solutions were also shown numerically to break into series of apparent solitary waves. An interesting property of the latter equation was that it seemed to possess solitary solutions formed by 'bumps' of vorticity riding on top of a uniform vortex layer. Although many types of waves of permanent form are known to exist on uniform vorticity layers, solitary waves have not been documented up to now, except for Pierrehumbert's touching dipole, which can be considered as a solitary wave whose thickness tends to zero at infinity.

In this paper we study the existence of families of solitary waves on vortex layers adjacent to walls, such that their heights do not vanish at infinity. We restrict ourselves

to layers of uniform vorticity, which allows us to use the formulation of contour dynamics. The computations in Jiménez & Orlandi (1993) were not restricted to uniform vorticity profiles, but the extra generality is not expected to be essential. The possible relation of these structures to near-wall turbulence will not be pursued here. The reader is referred to Orlandi & Jiménez (1991) and Jiménez & Orlandi (1993) for a discussion of those aspects.

Contour dynamics computations of time-evolving spatially periodic waves on a layer of uniform vorticity were carried out by Pullin (1981), motivated by their resemblance to the large-scale coherent motions in the outer part of constant-pressure turbulent boundary layers. The shapes and speeds of permanent periodic waves were computed by Broadbent & Moore (1985), which showed the existence of a finite limiting amplitude, comparable to the wavelength, characterized by sharp re-entrant corners in the wave troughs with an angle of 90°. Their results, as well as those of Pullin & Grimshaw (1983) for a related problem, strongly suggest that solitary waves may be found in the limit of long wavelengths. Pullin & Grimshaw (1988) computed the shape of solitary gravity waves in a flow with uniform shear, showing the transition from limiting profiles with a 120° corner at the crest, for small and moderate shear, to bubble-capped waves of probably unlimited amplitude for larger shear. Teles da Silva & Peregrine (1988) determined the shapes of large-amplitude periodic waves in this same configuration, and their results show a similar trend.

Perry & Fairlie (1975) used a similar model to mimic the recirculation bubble in a separating and reattaching turbulent boundary layer on the flat wall of a channel whose other wall was shaped to generate the necessary pressure distribution. They solved the inviscid equations by means of an electrical analogue technique, and found good agreement with their own wind tunnel experiments.

In §2 of this paper, we describe permanent solitary waves propagating on a two-dimensional layer of uniform vorticity. For small amplitudes, they approach solitons of the Benjamin–Ono equation, which arises as a limit of the equation proposed in Jiménez & Orlandi (1993). Waves of larger amplitude are described using contour dynamics. They tend to the Pierrehumbert dipole in the limit in which their amplitude is much larger than the thickness of the vorticity layer at infinity, and the nature of that limit is explored.

Solitary waves on a tube of azimuthal vorticity are described in §3, and their analogies and discrepancies with the planar waves are pointed out. It is conjectured that they may be related to the structures observed in turbulent jets. In the small-amplitude limit they tend to solitary waves of a slightly modified Korteweg–de Vries equation, and this connection might be related to the almost soliton-like behaviour observed experimentally in the interaction of coaxial vortex rings. In the large-amplitude limit they tend to Hill's spherical vortices.

The stability of the solutions is discussed briefly in §4, especially as it relates to the effect of weak viscosity and a no-slip wall. It is argued that the waves most probably separate the boundary layer and provoke vorticity ejections similar to those known to occur in the interaction of compact vortices with walls (Orlandi 1990).

2. Two-dimensional waves

We consider the propagation of two-dimensional waves on a layer of uniform vorticity adjacent to a slip wall in the absence of viscosity. Taking as units the values of the vorticity in the layer and its height, the unperturbed velocity field is

$$u_0 = \begin{cases} 1-y, & 0 < y < 1 \\ 0, & y > 1, \end{cases} \qquad v_0 = 0, \tag{1}$$

where y is the distance to the wall. The wave is characterized by the shape of the interface between rotational and irrotational fluid, $y = f(x, t)$.

The analysis of the evolution of infinitesimal waves, depending on x and t through a factor $\exp[ik(x-ct)]$, leads to the dispersion relation (Rayleigh 1887)

$$c = \frac{1}{2|k|}(1-\mathrm{e}^{-2|k|}), \tag{2}$$

which becomes $c = 1-|k|+\frac{2}{3}k^2+\ldots$ in the weakly dispersive limit of long wavelengths ($k \ll 1$).

For waves of small but finite amplitude, $y = 1+\epsilon F(x, t)$ with $\epsilon \ll 1$ and $F = O(1)$, a balance between the opposing tendencies of dispersion and nonlinearity is possible if $k_c = O(\epsilon)$, k_c being a characteristic wavenumber. Then, to leading order in an asymptotic expansion for $\epsilon \ll 1$, the waves obey the Benjamin–Ono equation (Benjamin 1967; Stern & Pratt 1985),

$$F_\tau + \frac{1}{\pi}\int_{-\infty}^{\infty} \frac{F_{\zeta'\zeta'}\,\mathrm{d}\zeta'}{\zeta'-\zeta} + FF_\zeta = 0, \tag{3}$$

where $\zeta = \epsilon(x-t)$, $\tau = \epsilon^2 t$, and the integral in the Hilbert's transform should be understood as a principal value. This equation has soliton solutions (Ablowitz & Clarkson 1991), which, in the original variables, are

$$f(x-ct) = 1+\frac{4\epsilon}{1+\epsilon^2(x-ct)^2}, \tag{4}$$

with

$$c = 1+\epsilon = 1+\tfrac{1}{4}[f(0)-1]. \tag{5}$$

We will now continue numerically this family of solitary waves for non-small values of the amplitude using contour dynamics. Guided by (4), we restrict our search to symmetric waves. In a reference frame moving with the unknown velocity of the wave, $\xi = x-ct$, we impose $f(-\xi) = f(\xi)$, and take $f(0)-1$ as a measure of the amplitude. The stream function describing the steady flow around the wave ($u = \psi_y$, $v = -\psi_x$, $\psi = 0$ at $y = 0$) is of the form

$$\psi(\xi, y) = \psi_0(y) - cy + \psi_b(\xi, y), \tag{6}$$

where

$$\psi_0(y) = \begin{cases} y(1-\frac{1}{2}y), & 0 < y < 1 \\ \frac{1}{2}, & y > 1 \end{cases} \tag{7}$$

is the stream function of the unperturbed flow. The perturbation can be split into

$$\psi_b(\xi, y) = \psi_+(\xi, y) + \psi_-(\xi, y), \tag{8}$$

with $$\psi_{\pm}(\xi,y) = \pm\frac{1}{2\pi}\int_{-\infty}^{\infty}\int_{1}^{f(\xi')} \ln\left[(\xi-\xi')^2+(y\mp y')^2\right]^{\frac{1}{2}} \mathrm{d}y'\,\mathrm{d}\xi'$$

$$= \frac{1}{2\pi}\int_{-\infty}^{\infty}\{I_{\pm}[\xi',f(\xi')]-I_{\pm}[\xi',1]\}\,\mathrm{d}\xi', \tag{9}$$

and $$I_{\pm}(\xi',y') = \ln\left[(\xi-\xi')^2+(y\mp y')^2\right]^{\frac{1}{2}}+y'+(\xi-\xi')\tan^{-1}\frac{y\mp y'}{\xi-\xi'},$$

where ψ_+ is the contribution to the stream function of the vorticity accumulated between $y=1$ and $y=f(\xi)$, and ψ_- that of its image relative to the wall.

For a solitary wave, with $f(\xi)\to 1$ for $\xi\to\pm\infty$, the condition that the boundary of the rotational region be a streamline is

$$\psi[\xi,f(\xi)] = \tfrac{1}{2}-c, \tag{10}$$

which provides an integral equation determining $f(\xi)$ and c as a function of $f(0)$.

In our numerical solution, (10) was imposed at $N+1$ discrete points ξ_i, $i=0,\ldots,N$, with $\xi_0=0$, and the integrals in (9) were approximated in terms of the values of $f(\xi)$ at these points using the trapeze rule. This yields $N+1$ equations for the unknowns, c and $f_i=f(\xi_i)$, $i=1,\ldots,N$. The spacing between adjacent points was chosen manually to provide some extra resolution at points of large curvature, but it was seldom very far from uniform. The length of the computational domain, ξ_N, was taken large enough for $f(\xi_N)-1$ to be negligible. The small contributions to the integrals from the regions beyond $\pm\xi_N$ were approximated by taking $f(\xi)=1+(f_N-1)(\xi_N/\xi)^2$ and expanding the integrands for ξ' large. This behaviour of $f(\xi)$ is associated with the vertical velocity $v\sim y/\xi^3$ far ahead of a vortex dipole, and is consistent with (4).

The discrete equations were solved iteratively using a simplified diagonal version of Newton's method introduced by Pierrehumbert (1980). The first equation ((10) at $\xi_0=0$) was used to compute c, and the others were iterated in the form

$$\psi^{(n)}(\xi_i,f_i^{(n)})+\left(\frac{\partial\psi^{(n)}}{\partial y}\right)_{(\xi_i,f_i^n)}\delta f_i^{(n)} = 0,$$

where the superscript denotes the iteration number and $\psi^{(n)}(\xi,y)$ is the value of ψ evaluated using $f^{(n)}$ in the integrals of $\psi_{\pm}$. The integral giving $\partial\psi_+/\partial y$ has a singular integrand at $\xi'=\xi_i$ and $y'=f(\xi_i)$, which was handled by separating the singular part and integrating it analytically over the interval $\xi_{i-1}<\xi<\xi_{i+1}$, using a linear approximation for $f(\xi)$.

The numerical continuation was initiated from $f(0)-1=0.1$, using the solution (4) of the Benjamin–Ono equation as an initial guess. The value of $f(0)-1$ was then increased by small steps, using the previously converged solutions as initial guesses. The length of the solitary wave was observed to first decrease (in accordance with the asymptotic results for $f(0)-1$ small) and then increase with increasing $f(0)$. The value of ξ_N was changed along the computation to accommodate these tendencies. Typically, N was about 200 and $\xi_N/f(0)\approx 8$, except for very small values of $f(0)-1$.

Values of the propagation speed and of the area Σ of the rotational region above the level $y=1$, are given in figure 1, normalized with $f(0)$ and $f(0)^2$. The dashed curve at the left of this figure corresponds to equation (5), whereas the area tends to 4π for $f(0)\to 1$, which agrees with the solution (4) of the Benjamin–Ono equation. Both the speed and the area increase monotonically with the amplitude of the wave, although

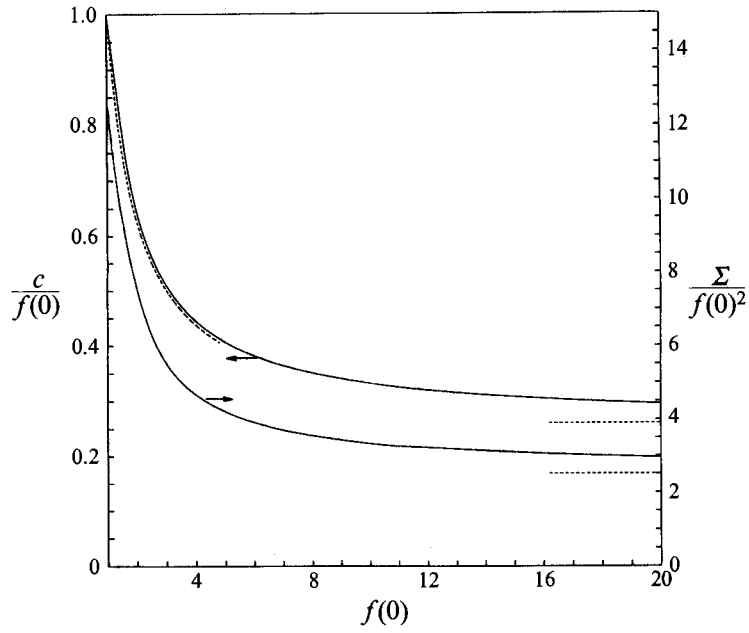

FIGURE 1. Normalized propagation speed and area of the rotational region above the level of the unperturbed vorticity layer for a planar wave, as functions of its amplitude. The dashed curve to the left of the figure is equation (5), and the dashed lines to the right are the asymptotic Pierrehumbert's results for large amplitude.

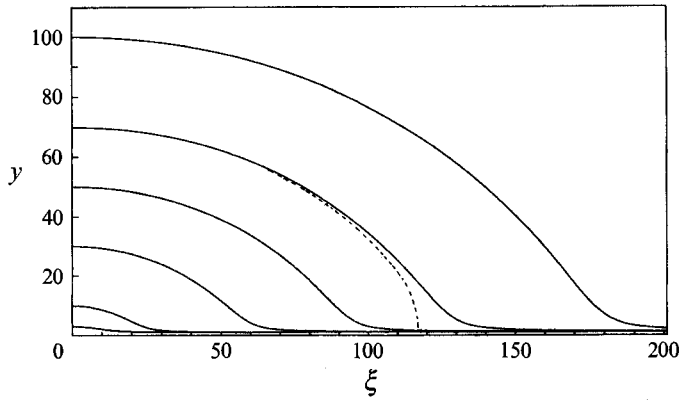

FIGURE 2. Shapes of the planar waves for six different amplitudes. The dashed curve gives the shape of Pierrehumbert's vortex.

their normalized values decrease. The horizontal lines at the right of the figure are $c/f(0) = 0.26$ and $\Sigma/f(0)^2 = 2.51$, corresponding to the speed and area of the limiting touching member of Pierrehumbert's (1980) family of pairs of counter-rotating vortices. One vortex of the dipole corresponds to our solitary wave, while the other is provided by the image vorticity on the other side of the slip wall. The present results tend asymptotically to that limit as $f(0)$ increases and the uniform vortex layer extending to infinity is overwhelmed by the vorticity in the wave. This tendency is also reflected in figure 2, which displays the wave shapes for several amplitudes; the dashed line is the limiting Pierrehumbert solution for a half-height equal to 70.

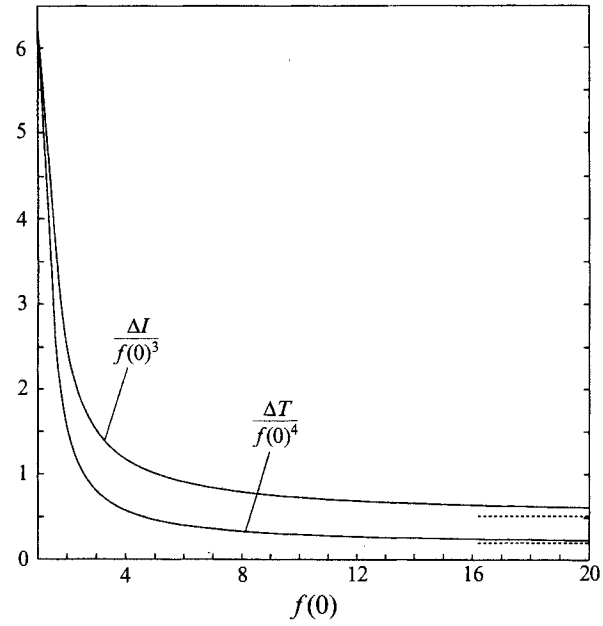

FIGURE 3. Normalized excesses of impulse and energy of a planar wave as functions of its amplitude. The dashed lines are the asymptotic results for Pierrehumbert's vortex.

Figure 3 shows the excesses of the ξ-component of the impulse ΔI and of the kinetic energy ΔT of the waves above the values of the unperturbed flow. The quantities themselves are infinite, but the excesses are finite, and are given by

$$\Delta I = \frac{1}{2}\int_\Sigma y\,\mathrm{d}\xi\,\mathrm{d}y = \frac{1}{4}\int_{-\infty}^{\infty}(f^2-1)\,\mathrm{d}\xi$$

and

$$\Delta T = -\frac{1}{2}\int_\Sigma (\psi_0+\psi_b)\,\mathrm{d}\xi\,\mathrm{d}y + \frac{1}{2}\int_{0\leqslant y\leqslant 1}\psi_b\,\mathrm{d}\xi\,\mathrm{d}y$$

$$= -\frac{1}{4}\int_{-\infty}^{\infty}\left\{\frac{f^3-1}{3}-(f-1)(2cf+1)+f^2\left(\frac{\partial\psi}{\partial y}+c\right)\right\}\mathrm{d}\xi.$$

Note that the infinite contribution to the energy excess due to the circulation of the wave is cancelled by the opposite circulation of its image relative to the wall. In the second expression, ΔT has been reduced to a line integral through integration by parts and the use of Green's identities, and $\partial\psi/\partial y$ is evaluated at the boundary of the rotational region. The excesses of impulse and energy increase with increasing amplitude from the common value 2π, for $\epsilon \ll 1$, to the asymptotic Pierrehumbert's values $\Delta I = 0.516 f(0)^3$ and $\Delta T = 0.20 f(0)^4$ for large amplitudes (dashed lines in figure 3).

Pierrehumbert's vortex is not retrieved uniformly, however, in the limit of large amplitudes. The extent of the rotational region is finite in Pierrehumbert's solution and, as proved by Saffman & Tanveer (1982), its boundary meets the symmetry plane ($y = 0$) at right angles, although with infinite curvature (see also Wu, Overman & Zabusky 1984), whereas in our case a layer of vorticity extends to infinity ahead and behind the vortex, and the interface tends asymptotically to $y = 1$. Far from the vortex, this layer behaves in a passive way, since the translation velocity of the vortex, $O[f(0)]$, is much larger than the velocity difference across the layer, which is $O(1)$. The same is

true over most of the periphery of the vortex. The flow velocity is $O[f(0)]$, and the vorticity coming from infinity occupies a layer whose thickness is $O(1)$, inducing velocities which are small compared to the induction of the bulk of the vortex. However, there are small regions of size $O[f(0)]^{\frac{1}{2}}$, near the front and back tips of the vortex, where the velocity induced by the vorticity coming from the layer at infinity becomes comparable with that induced by the rest of the vortex. It is in these regions that the shape and velocity field of the present solution tend very slowly to those of Pierrehumbert.

We discuss now the structure of the flow in the region near the leading tip of the vortex. The flow around the rear is analogous. Note that, up to logarithms, the magnitude of the velocity in the Saffman & Tanveer (1982) solution for the Pierrehumbert vortex decreases linearly to zero near the tip, which is a stagnation point, $q = O(|\xi - 3.34f(0)|)$ (see (11) and (12) below). The height of the rotational strip coming from infinity increases in inverse proportion to this velocity, as $f(0)/q$, and the velocities induced by the vorticity contained in the strip increase proportionally to its height. Hence, the two velocities become comparable when $q = O[f(0)]^{\frac{1}{2}}$, and the incoming vorticity, which by then has accumulated in a non-slender region of size $O[f(0)]^{\frac{1}{2}}$, around the tip of the vortex, begins to play a role in the local dynamics.

Let us call $[f(0)]^{\frac{1}{2}} = \beta \gg 1$, and define polar coordinates (r, θ) centred at $\xi = 3.34\beta^2$, $y = 0$, which would be the leading tip of a touching Pierrehumbert pair whose half-height was β^2 (see figure 4, where the boundary of Pierrehumbert's vortex is represented by the dashed line, and the solid line represents the boundary of the present vortex). The stream function in the potential and rotational regions, ψ_1 and ψ_2, and the vortex boundary $\theta = \theta_b(r)$, are given for the Pierrehumbert dipole, at $r \ll \beta^2$, by equation (1)–(3) of Saffman & Tanveer (1982), which can be rewritten as

$$\psi_1 = \mathrm{Im}\left\{z^2\left(\frac{\ln(z/\beta^2)}{2\pi} + \alpha\right)\right\} + O\left(\frac{r^2}{\ln(r/\beta^2)}\right), \tag{11}$$

$$\psi_2 = -\frac{r^2}{2}\cos^2\theta + \mathrm{Im}\left\{z^2\left(\frac{\ln(z/\beta^2)}{2\pi} + \alpha\right)\right\} + O\left(\frac{r^2}{\ln(r/\beta^2)}\right), \tag{12}$$

$$\theta_b = \frac{\pi}{2} - \frac{\pi/4}{\ln(r/\beta^2)} + O\left(\frac{1}{(\ln(r/\beta^2))^2}\right), \tag{13}$$

where $z = re^{i\theta}$, α is a real constant (≈ -0.13 according to Turfus (1993), who also computed some further terms of the expansions (11)–(13)), and the branch cut of the logarithm is taken along the negative ξ-axis.

The first deviation of the present vortex from the shape (13) is due to the non-zero value of the stream function on the boundary of the rotational region. While in Pierrehumbert's case the stream function vanishes both at the wall and at the boundary of the vortex, here it is only zero at the wall, and equals $-\beta^2 U + \frac{1}{2}$ (with $U = c/\beta^2 = 0.26$) on the boundary. Using this condition, (11) and (12) yield the corrected shape

$$\theta_b(r) = \frac{\pi}{2} - \frac{\pi/4 - \beta^2\pi U/r^2}{\ln(r/\beta^2)}\left[1 + O\left(\frac{1}{\ln(r/\beta^2)}\right)\right]. \tag{14}$$

Thus, the inverse-logarithm decay of $\theta - \frac{1}{2}\pi$ near the tip of Pierrehumbert's vortex changes to an algebraic decay for $r = O(\beta)$. This expansion is valid for $r \ll \beta^2$ and $|\theta_b - \frac{1}{2}\pi| \ll 1$, as long as the value of the stream function at the boundary, which is $O(\beta^2)$, remains small compared to the characteristic value of the stream functions at

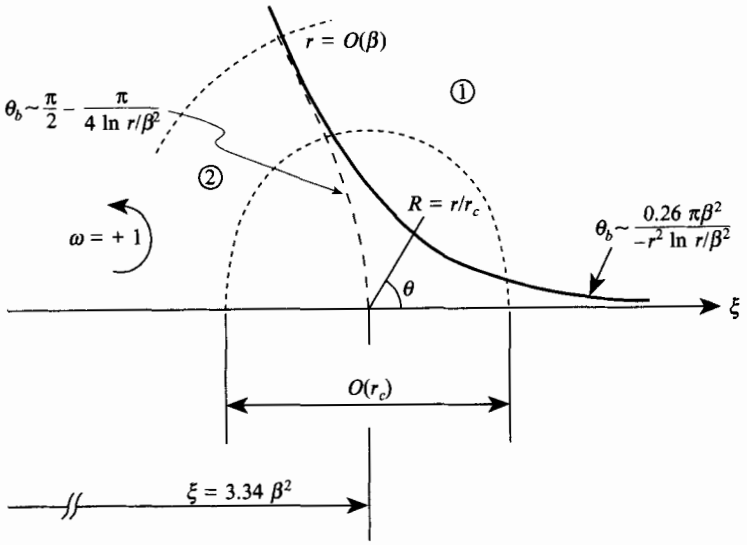

FIGURE 4. Sketch of the region near the leading tip of a planar wave of very large amplitude.

comparable distances from the tip. According to (11) and (12), both values become comparable for $R \equiv r/r_c = O(1)$, with $-r_c^2 \ln(r_c/\beta^2) = \beta^2$, which defines the limit of an inner region that has to be treated separately. Note that $r_c \approx \beta/(\ln\beta)^{\frac{1}{2}} \ll \beta$, at least formally, and that the term in (14) proportional to $-\beta^2/r^2$ is dominant over the one proportional to $\frac{1}{4}\pi$ in the inner end of the intermediate region.

In this inner region the dominant contribution to the stream function is still the stagnation point flow induced by the rest of the vortex, which is given by the common $O(\beta^2)$ leading term of the outer solutions (11) and (12), while the contribution of the local vortical fluid to the stream function is only $O(r^2) = O(r_c^2)$. The inner expansions for the stream functions are therefore of the form

$$\psi_1 = -\beta^2 \frac{R^2 \sin 2\theta}{2\pi} + r_c^2 \overline{\psi_1} + O\left(\frac{r_c^2}{\ln(r_c/\beta_2)}\right), \tag{15}$$

$$\psi_2 = -\beta^2 \frac{R^2 \sin 2\theta}{2\pi} + r_c^2 \overline{\psi_2} + O\left(\frac{r_c^2}{\ln(r_c/\beta^2)}\right), \tag{16}$$

where
$$\nabla_I^2 \overline{\psi_1} = 0, \quad \nabla_I^2 \overline{\psi_2} = -1, \tag{17a, b}$$

and ∇_I^2 is the Laplacian in the inner variables (R, θ). The asymptotic forms of $\overline{\psi_1}$ and $\overline{\psi_2}$ for $R \gg 1$, are

$$\overline{\psi_1} \sim \mathrm{Im}\left\{Z^2\left(\frac{\ln Z}{2\pi} + \alpha\right)\right\}, \tag{18a}$$

and
$$\overline{\psi_2} \sim \overline{\psi_1} \qquad \text{for} \quad \theta \ll 1, \tag{18b}$$

$$\overline{\psi_2} \sim -\frac{R^2}{2}\cos^2\theta + \mathrm{Im}\left\{Z^2\left(\frac{\ln Z}{2\pi} + \alpha\right)\right\} \quad \text{for} \quad \theta = O(1), \tag{18c}$$

where $Z = z/r_c$. Here (18a) and (18c) are the forms of the outer solutions (11) and (12) rewritten in terms of R and θ. The different behaviour of $\overline{\psi_2}$ to the left and to the right of the inner region reflects the fact that the effect of the incoming vorticity is important to this order for the flow on the left, but not on the right, over the passive tail.

Finally, the inner expansion of the boundary of the vortex, $R = R_b(\theta)$ is of the form

$$R_b = R_0(\theta) + \frac{R_1(\theta)}{\ln(r_c/\beta^2)} + O\left(\frac{1}{(\ln(r_c/\beta^2)^2}\right), \tag{19}$$

where R is written here as a function of θ on the boundary because the alternative representation $\theta = \theta_b(R)$ leads to a multi-valued function (see figure 4). The boundary is defined by the conditions $\psi_1 = \psi_2 = -\beta^2 U + \frac{1}{2}$ and $\psi_{1\theta} = \psi_{2\theta}$. Inserting (19) into (15) and (16), applying these conditions, and separating like-order terms of the expansions, we find

$$R_0(\theta) = \left(\frac{2\pi U}{\sin 2\theta}\right)^{\frac{1}{2}}, \tag{20}$$

and

$$\frac{R_0(\theta)\, R_1(\theta) \sin\theta}{\pi} + \overline{\psi_i}[R_0(\theta), \theta] = 0, \quad i = 1, 2, \tag{21a, b}$$

$$\overline{\psi_{1\theta}}[R_0(\theta), \theta] = \overline{\psi_{2\theta}}[R_0(\theta), \theta]. \tag{21c}$$

Note that the leading term of the expansion of (14) for $r/\beta \ll 1$ coincides with that of (20) for $\theta \nearrow \frac{1}{2}\pi$. This can be easily verified writing $r = r_c R$, decomposing the logarithm in (14) and using the definition of r_c, and expanding the sine in (20). At the other limit, $r/\beta \gg 1$, (14) tends to (13), providing a connecting expansion valid in the range $r_c \ll r \ll \beta^2$. Note also that no intermediate region of $r = O(\beta)$ is required to the right of the inner region, at least to the order of the present computation. There, the behaviour $\theta_b \sim -\beta^2 \pi U / r^2 \ln(r/\beta^2)$, obtained by setting ψ_1 in (11) equal to $-\beta^2 U$ for $\theta \ll 1$, remains valid for any $r_c \ll r \ll \beta^2$, and is continued by the streamline $\psi_1 = -\beta^2 U$ of the outer Pierrehumbert's flow, beyond the range of validity of (11).

Equations (17*a*, *b*), (18*a–c*), and (21*a–c*), along with the conditions $\overline{\psi_2} = 0$ at $\theta = 0$ and π, determine $\overline{\psi_1}$, $\overline{\psi_2}$, and θ_1. Contrary to the original problem, this is not a free boundary problem. The conditions (21*a–c*) imply the continuity of the $\overline{\psi_i}$ and of their first derivatives at the line $R = R_0(\theta)$, which is already known from (20). The two functions $\overline{\psi_1}$ and $\overline{\psi_2}$ are the unique solution of a standard boundary value problem, and $R_1(\theta)$ is computed from (21*a*) or (21*b*) only after the $\overline{\psi_i}$ are determined. In principle, the same procedure can be applied to the higher-order terms of the expansion (which contains further logarithms and their iterates in a far from trivial ordering) and a formal test of consistency of the asymptotic structure can thereby be obtained. This is probably more important than the practical use of the asymptotic expansion to evaluate the solution near the tip, because the expansion is hampered in this respect by the presence of logarithms.

3. Axisymmetric waves

Calculations analogous to those of the previous section can be carried out for axisymmetric solitary waves propagating on a vortical tube with azimuthal vorticity confined to a cylindrical region in an otherwise irrotational fluid without swirl. We assume that the magnitude of the vorticity is proportional to the distance to the symmetry axis. This property is maintained by the dynamics of the inviscid fluid. We note, however, that many of the results corresponding to small-amplitude waves hold, with minor changes, for other vorticity distributions, both in this and in the two-dimensional case (see Jiménez & Orlandi 1993).

Taking the radius of the unperturbed rotational region and the maximum vorticity as units, the unperturbed flow is

$$(\omega, u_0, \psi_0) = \begin{cases} [r, & \frac{1}{2}(1-r^2), & \frac{1}{4}(1-\frac{1}{2}r^2)\,r^2], & 0<r<1 \\ (0, & 0, & \frac{1}{8}), & r>1, \end{cases} \tag{22}$$

where ω, u, and ψ are respectively the azimuthal vorticity, the axial (x) velocity, and the Stokes stream function, defined by $u = \psi_r/r$, $v = -\psi_x/r$, $\psi = 0$ at $r = 0$.

The dispersion relation for infinitesimal axisymmetric waves propagating in this medium is

$$c = -|k|\,K_0'(|k|)\int_0^1 \eta I_0(|k|\,\eta)\,\mathrm{d}\eta, \tag{23}$$

where K_0 and I_0 are the modified Bessel functions of order zero. In the limit of long waves, (23) reduces to $c = \frac{1}{2}+\frac{1}{4}(\frac{1}{2}\ln|k|+\gamma-\frac{1}{4})k^2+\ldots$, where $\gamma = 0.5772\ldots$ is Euler's constant.

A balance of dispersion and nonlinearity for small-amplitude waves occurs now for $k_c = O(\epsilon^{\frac{1}{2}})$ (up to logarithms), where, as before, $\epsilon = f(0)-1$ is the amplitude of the wave. Writing the shape of the boundary in the form $r = 1+\epsilon F(\zeta,\tau)$, where $\zeta = \epsilon^{\frac{1}{2}}(x-\frac{1}{2}t)$ and $\tau = \epsilon^{\frac{3}{2}}t$, the equation giving $F(\zeta,\tau)$ for $\epsilon \ll 1$ can be easily found to be

$$F_\tau+\tfrac{1}{4}(-\ln(\tfrac{1}{2}\epsilon^{\frac{1}{2}})-\gamma+\tfrac{1}{4})F_{\zeta\zeta\zeta}-\frac{1}{4}\frac{\partial^3}{\partial\zeta^3}\left\{\int_{-\infty}^{\infty}\ln|\kappa|\,\hat{F}(\kappa,\tau)\,\mathrm{e}^{\mathrm{i}\kappa\zeta}\,\mathrm{d}\kappa\right\}+FF_\zeta = 0, \tag{24}$$

where $\hat{F}$ is the Fourier transform of F. Equation (24) was obtained by Leibovich (1970) in the context of weakly nonlinear waves propagating in rotating fluids. Leibovich & Randall (1972) found numerically that (24) has solitary wave solutions which, when $-\ln\frac{1}{2}\epsilon^{\frac{1}{2}} \gg 1$, differ very little from the solitons of the KdV equation, to which (24) reduces, after appropriate rescaling, in the limit $\epsilon \to 0$. The propagation speed of these waves, written in the original variables, is

$$c = \tfrac{1}{2}+\frac{f(0)-1}{2}\left[1+O\left(\frac{1}{-\ln[f(0)-1]}\right)\right], \tag{25}$$

and the volume of the rotational region with $r > 1$ is

$$V = 8\sqrt{2}\,\pi\left(-\ln\frac{(f(0)-1)^{\frac{1}{2}}}{2}-\gamma+\tfrac{1}{4}\right)^{\frac{1}{2}}(f(0)-1)\left[1+O\left(\frac{1}{-\ln[f(0)-1]}\right)\right]. \tag{26}$$

As for the two-dimensional case, we proceed now to extend the solitary wave solutions of (24) to non-small amplitudes using contour dynamics. For this purpose, the Stokes stream function in a reference frame moving with the wave ($\xi = x-ct$) is written as

$$\psi(\xi,r) = \psi_0(\xi,r)-\tfrac{1}{2}cr^2+\psi_b(\xi,r), \tag{27}$$

where, again, ψ_b is the contribution of the extra vorticity concentrated in the wave. It can be expressed as a volume integral extended to the toriodal region enclosed between the surface of the wave, $r = f(\xi)$, and the cylinder $r = 1$, and Shariff, Leonard & Ferziger (1989) showed that it can be transformed into a line integral over the contour of a meridional cross-section of the torus. In our notation:

$$\psi_b = \frac{r}{4\pi}\int_{-\infty}^{\infty}\left\{(\xi-\xi')\,I_2\frac{\mathrm{d}r'}{\mathrm{d}\xi'}+r'I_2-rI_3\right\}r'^2\,\mathrm{d}\xi-\frac{r}{4\pi}\int_{-\infty}^{\infty}(I_2-rI_3)\,\mathrm{d}\xi', \tag{28}$$

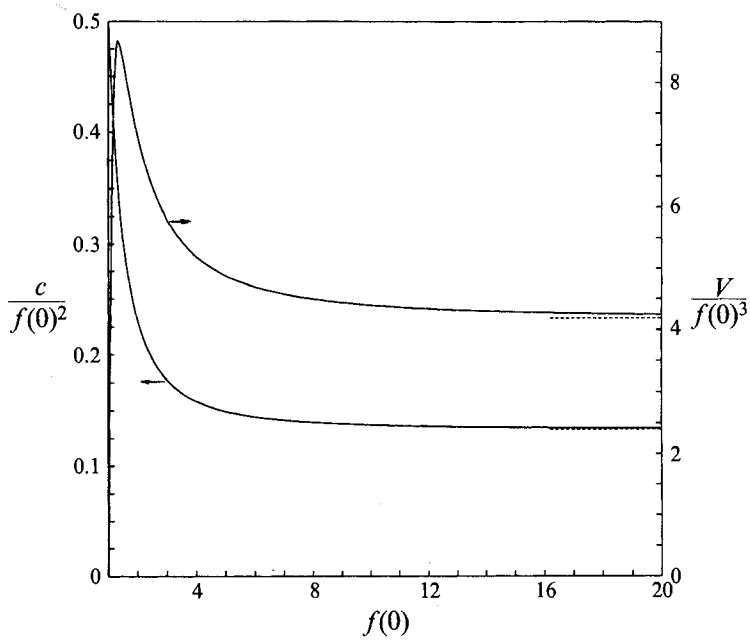

FIGURE 5. Normalized propagation speed and volume of the rotational region outside the unperturbed vortical tube for an axisymmetric wave as functions of its amplitude. The dashed lines are the asymptotic values corresponding to the Hill vortex.

where

$$I_1 = \frac{2}{(A+B)^{\frac{1}{2}}}K(m), \quad I_2 = \frac{A}{B}I_1 - \frac{2}{B}(A+B)^{\frac{1}{2}}E(m), \quad I_3 = \frac{1}{3}\left(4\frac{A}{B}I_2 - I_1\right)\Bigg\} \tag{29}$$
$$m = 2B/(A+B), \quad A = (\xi-\xi')^2 + r^2 - r'^2, \quad B = 2rr';$$

$K(m)$ and $E(m)$ are the complete elliptic integrals of the first and second kind, respectively, and m is their modulus. In the first integral of (28) $r' = f(\xi')$, whereas $r' = 1$ in the expressions for the Is appearing in the second integral.

As before, we look for symmetric waves with a maximum at $\xi = 0$, and take $f(0) - 1$ as a measure of the amplitude. The condition

$$\psi[\xi, f(\xi)] = \tfrac{1}{8} - \tfrac{1}{2}c, \tag{30}$$

imposed at $N+1$ points, $\xi_0 = 0$ to ξ_N, provides $N+1$ equations for the unknowns $f_i = f(\xi_i)$, $i = 1, \ldots, N$, and c. These equations are discretized and solved by the same iterative scheme used before, which involves the value of $(\partial\psi/\partial r)_{(\xi_i, f_i)}$. The contribution of ψ_b to this derivative is (Shariff *et al.* 1989)

$$\frac{\partial\psi_b}{\partial r} = \frac{r}{2\pi}\int_{-\infty}^{\infty}\left\{(\xi-\xi')I_1\frac{\mathrm{d}r'}{\mathrm{d}\xi'} - rI_2\right\}r'\,\mathrm{d}\xi' + \frac{r^2}{2\pi}\int_{-\infty}^{\infty} I_2\,\mathrm{d}\xi'. \tag{31}$$

The integrand of (28) is regular, while that of (31) has a logarithmic singularity at $\xi' = \xi_i$ and $r' = f(\xi_i)$ (in (30) at $\xi = \xi_i$). The singular part of this integrand is isolated and integrated analytically over the two intervals adjacent to $\xi' = \xi_i$ using a linear approximation for $f(\xi)$. The asymptotic expression $f(\xi) = 1 + (f_N - 1)|\xi_N/\xi|^3$ is used in the integrals for $|\xi'| > \xi_N$.

The propagation speed and the volume of the rotational region outside $r = 1$ are represented in figure 5 as functions of $f(0)$. As can be seen, the speed tends to $\frac{1}{2}$ and the volume tends to zero for $f(0) \to 1$, in accordance with (25) and (26). The dashed lines

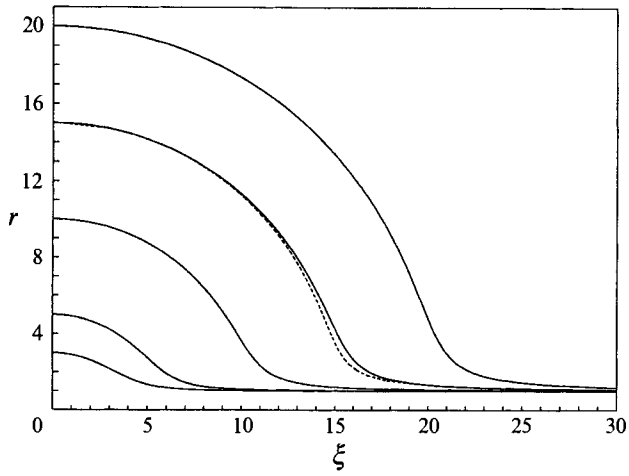

FIGURE 6. Shapes of the axisymmetric waves for five different amplitudes. The dashed curve is the streamline of a Hill vortex that tends to $r = 1$ far from the vortex.

at the right of the figure are the speed and volume of Hill's spherical vortex: $c/f(0)^2 = \frac{2}{15}$ and $V/f(0)^3 = \frac{4}{3}\pi$, to which the present results tend for $f(0)$ large. The shapes of the waves for several values of $f(0)$ are given in figure 6.

Comparison of figures 1 and 5 shows that the scaled velocity and area (or volume) of the waves tend to their large-amplitude limits more rapidly in the axisymmetric case than in the planar case, and the same is true of the shapes of the waves (specially near the tips). This is connected with the more passive role of the vorticity of the incoming fluid in the axisymmetric case when the wave amplitude increases, so that, for a given (large) amplitude, these waves are closer to Hill spherical vortices that the planar waves are to Pierrehumbert vortices. An estimate of the effect of this vorticity in comparison with that of the vorticity accumulated in the wave is given at the end of this section.

The expressions for the excesses of axial impulse and energy are, after some manipulation,

$$\Delta I = \frac{\pi}{4}\int_{-\infty}^{\infty} (f^4 - 1)\,\mathrm{d}\xi$$

and

$$\Delta T = -\frac{\pi}{16}\int_{-\infty}^{\infty} \left\{\frac{f^6-1}{3} - (f^2-1)(4cf^2+1) + 2f^3\left(\frac{\partial\psi}{\partial r} + cf\right)\right\}\mathrm{d}\xi,$$

with $\partial\psi/\partial r$ evaluated at the boundary of the rotational region. These quantities are represented in figure 7. As for the two-dimensional case, both increase monotonically with the amplitude of the wave, going from zero when $f(0) \to 1$ to the asymptotic behaviour $\Delta I = (4\pi/15)f(0)^5$ and $\Delta T = (8\pi/315)f(0)^7$ (corresponding to Hill's vortex) for large amplitudes.

The shape of the wave for $f(0) \to \infty$ tends fairly rapidly to a streamline of the flow around a Hill vortex of radius $f(0)$. As for the two-dimensional case, we restrict ourselves to the analysis of the leading tip of the vortex. The velocity of the incoming fluid with respect to the stationary wave, which is $O[f(0)^2]$ away from the vortex, decreases near the stagnation point as $q \sim f(0)\,|\xi - f(0)|$, so that the radius of the incoming vortical tube increases as $[f(0)^2/q]^{\frac{1}{2}}$. At the same time, the vorticity in the tube is stretched to $\omega \sim r$ and the velocity induced by it increases as $q_I \sim \omega r \sim f(0)^2/q$. These estimates hold until the incoming vortical fluid reaches a distance to the stagnation

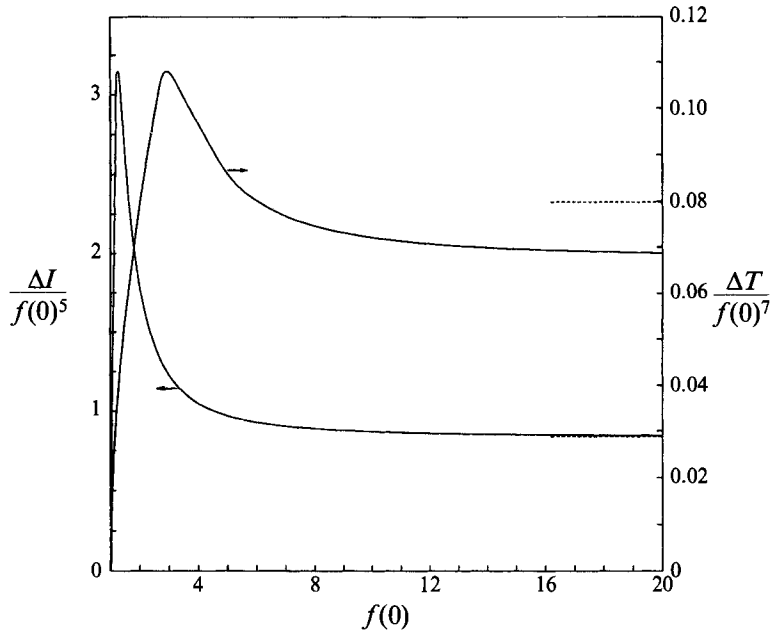

FIGURE 7. Normalized impulse and energy of an axisymmetric wave as functions of its amplitude. The dashed lines are the asymptotic values corresponding to the Hill vortex.

point which is comparable with its own radius, at which point the cylindrical approximation cannot be used any more, the tube splits into an annulus, and its thickness starts to decrease. It is easy to see that the maximum induced velocity occur at this point, where $|\xi - f(0)| \sim f(0)^{\frac{1}{3}}$. The induced velocity there is $q_I \sim f(0)^{\frac{2}{3}}$, while the velocity generated by the bulk of the wave is larger, $q \sim f(0)^{\frac{4}{3}}$. As a consequence, the incoming vorticity plays a passive role everywhere, and the boundary of the vortex tends to the streamline $\psi = -f(0)^2/15$ of the flow around a Hill vortex. The dashed line in figure 6 represents this streamline for $f(0) = 15$. The agreement with the computed boundary is already good for this moderate value of $f(0)$, and becomes better as $f(0)$ increases.

4. Discussion

The axisymmetric waves of small enough amplitude are most probably stable, since they a very close to solitons of the KdV equation (Leibovich & Randall 1972). Waves of large enough amplitude must be unstable, since they tend to a Hill vortex, which is known to be unstable (Bliss 1973; Moffatt & Moore 1978; Pozrikidis 1986). Therefore, at least one critical amplitude must exist at which the waves change stability. The instability of Hill's vortex leads to the ejection of vorticity from the rear of the vortex if the initial perturbation is prolate, and to the ingestion of irrotational fluid if the perturbation is oblate. It would be of some interest to find how these processes are modified by the presence of the tube of vortical flow, and to see whether the short-wave undulations of the vortex surface predicted by Bliss (1973) and Shariff *et al.* (1989) also appear in this case.

The planar waves of small amplitude are also solitons (see e.g. Ablowitz & Clarkson 1991). Less is known about the stability of the touching pair of counter-rotating vortices, but it is generally supposed to be stable (see comments in Saffman 1993 and

Saffman & Szeto 1980). If this is so, the solitary waves of §2 might be stable for all amplitudes.

It is interesting to note that the finite waves that we have described always contain a recirculation bubble adjacent to the wall (or to the axis). In the weak planar case, the velocity at the wall relative to the wave is given asymptotically by

$$u(\xi, 0) = \epsilon\left(1 - \frac{4}{1+\epsilon^2\xi^2}\right), \tag{32}$$

where ϵ is the amplitude parameter $f(0) - 1$. This velocity vanishes at $\xi = \pm\sqrt{3}/\epsilon$, and reverses direction between those two stagnation points. The streamline connecting them defines a recirculation bubble that increases in size and intensity as the waves become stronger and the stagnation points move towards the tips of the Pierrehumbert vortex. The recirculation region was noted by Teles da Silva & Peregrine (1988) for the high shear limit of their waves and is a common feature of many strong vorticity waves.

Although the analysis in this paper is inviscid, the effect of viscosity when the waves move along a no-slip wall merits some comment. The velocity distribution in equation (32) is the same as that generated by a point vortex moving at some distance from a wall under its own induction. The boundary layer generated by that flow was studied by Doligalski & Walker (1984), who concluded that it always separates a little downstream from the pressure minimum located underneath the vortex. Since the boundary-layer behaviour depends only on the velocity distribution along its edge, their conclusions remain valid here, and hold for all wave amplitudes. The somewhat counterintuitive conclusion that an arbitrarily small Benjamin–Ono soliton will separate the boundary layer is explained because its small amplitude, ϵ, is compensated by its long wavelength, $O(1/\epsilon)$. The nature of the separation, in the point-vortex case, is that some of the vorticity is ejected from the boundary layer. A similar phenomenon was observed by Jiménez (1990) underneath the finite-amplitude Tollmien–Schlichting waves in a two-dimensional channel. In that case the boundary layer separates near the rear stagnation point of the wave, forming a thin vortex layer which wraps around the main vortex. The process is not particularly violent and is even steady with respect to the wave at sufficiently small Reynolds numbers. Doligalski & Walker (1984) suggest that this ejection process might be related to the bursting phenomenon in turbulent boundary layers. In our conceptual model, in which the waves would correspond to streamwise vortices, the separated layers would form vorticity 'walls' oriented parallel to the stream. Such wrapped shear layers have been documented in turbulent channels in Jiménez & Moin (1991).

Although this discussion holds strictly only for the velocity distribution (32), generated by weak waves, it can be checked numerically that the pressure gradients induced by strong waves are even more unfavourable than in the weak case.

The results of this paper might also be used to discuss the viscous decay of freely propagating laminar vortex pairs (or rings). If the Reynolds number based on the half-height of the pair (H) and on its propagation velocity (U) is large, a diffusion layer of characteristic thickness $\delta = O(H/Re^{\frac{1}{2}})$ appears on the periphery and near the symmetry axis of the vortex pair, as the vorticity diffuses away from the rotational region or gets cancelled by vorticity of the opposite sign. Some fraction of this vorticity would be left behind the vortices, giving rise to a wake. This would be analogous to the infinite vorticity layer (or tube) considered above, which would now only exist on the back of the pair, whereas the flow in the other side would resemble that of Pierrehumbert's or Hill's solutions. In this analogy, the relative height of the vortex, $f(0)$, would be a quantity of order $Re^{\frac{1}{2}} \gg 1$ with respect to the wake, but the structure of the corner

region at the rear of the vortex would be more complex than the one discussed in §2 because, although the viscosity does not play a direct dynamical role in this region, the vorticity (or ω/r in the axisymmetric case) coming from the diffusion layer is not uniform.

The thickness and distribution of this layer depends on how much mass is lost to the wake together with the vorticity. If a sizeable fraction of the diffusion layer is lost in this way, the vorticity in the core (or ω/r) might remain essentially constant throughout the decay. In this case, the rate of mass loss would be of order $U\delta$ in the planar case (resp. $UH\delta$ in the axisymmetric case), leading to $\mathrm{d}H/\mathrm{d}t = O[(\nu\omega)^{\frac{1}{2}}]$ (resp. $\mathrm{d}H/\mathrm{d}t = O[(\mathscr{A}H)^{\frac{1}{2}}]$), where ν is the kinematic viscosity, ω is the vorticity in the interior of the vortex (resp. $\mathscr{A} = \omega/r$), and where use has been made of the estimate $U = O(\omega H)$ [resp. $U = O(\mathscr{A}H^2)$]. These results imply a finite lifetime for the vortex pair, of the order of $Re^{\frac{1}{2}}$ eddy turnover times.

On the other hand the vortex pair might entrain most of the diffusion layer, including fluid that was originally irrotational, as it actually happens in the vortex ring. This would be specially true if the loss of total head of the outer fluid through friction is enough to prevent it from reaching the rear stagnation point. The decay process would then be more complex, involving the sharing of the available vorticity by the ever-increasing amount of fluid in the vortex, and no simple estimate is possible in the absence of more detailed computations or experiments (see Maxworthy 1972, 1974 and Shariff & Leonard 1992 for a discussion of the decay of a vortex ring). At first sight, the newly entrained fluid would orbit in an outer region around the rotational core, which would split into two disconnected parts (or become a torus in the axisymmetric case). This outer region has some vorticity, and the possibility of a continued entrainment depends on it. This would leads to a very slow decay, for the viscous diffusion would have to extend to a considerable part of the vortex. Which of these possibilities are realized, how large is the diffusion layer, and what is its structure, are issues that cannot be decided without further analysis.

5. Conclusions

A family of solitary waves propagating on a layer of uniform vorticity adjacent to a slip wall in an otherwise stagnant fluid have been bound by a combination of perturbation methods, for small-amplitude waves, and contour dynamics for larger amplitudes. These waves are concentrations of vorticity behaving as counter-rotating dipoles under the influence of their images relative to the wall, and correspond to the structures observed in numerical simulations of a related initial value problem in Jiménez & Orlandi (1993). Their propagation speed, area, and excesses of impulse and kinetic energy relative to the unperturbed flow, have been computed as functions of the amplitude. An asymptotic analysis is presented for very strong waves, which tend almost everywhere to one of the partners of the touching pair of counter-rotating vortices computed by Pierrehumbert (1980). Weak wave approximate solitons of the Benjamin–Ono equation. Permanent periodic waves in a vorticity layer had been described previously by Broadbent & Moore (1985), and it is almost certain that our solitary waves correspond to the long-wave limit of their solutions.

It is argued, by analogy to the flow induced by a point vortex, that these waves separate the boundary layer induced by them over a no-slip wall, most probably resulting in the ejection of a concentrated vortex layer into the flow.

A similar family of axisymmetric solitary waves is also found for a tube of azimuthal vorticity immersed in a fluid at rest. These waves range from solitons of the KdV

equation, for very small amplitudes, to the Hill's spherical vortex for amplitudes large compared to the radius of the vorticity tube.

This work was supported in part by the CICYT, under grants NAT 91-02220C04-02, ESP 187/90 and PB92-1075. We have benefitted from discussions with K. Shariff.

REFERENCES

ABLOWITZ, M. J. & CLARKSON, P. A. 1991 *Solitons, Nonlinear Evolution Equations, and Inverse Scattering*. Cambridge University Press. Pp. 173–181.

BENJAMIN, T. B. 1967 Internal waves of permanent form in fluids of great depth. *J. Fluid Mech.* **29**, 559–592.

BLISS, D. B. 1973 The dynamics of flows with high concentration of vorticity. PhD thesis, Dept. Aero. & Astro., MIT.

BROADBENT, E. G. & MOORE, D. W. 1985 Waves of extreme form on a layer of uniform vorticity. *Phys. Fluids* **28**, 1561–1563.

DOLIGALSKI, T. L. & WALKER, J. D. A. 1984 The boundary layer induced by a convected two-dimensional vortex. *J. Fluid Mech.* **139**, 1–28.

JIMÉNEZ, J. 1990 Transition to turbulence in two-dimensional Poiseuille flow. *J. Fluid. Mech.* **218**, 265–297.

JIMÉNEZ, J. & MOIN, P. 1991 The minimal flow unit in near-wall turbulence. *J. Fluid Mech.* **225**, 213–240.

JIMÉNEZ, J. & ORLANDI, P. 1993 The roll-up of a vortex layer near wall. *J. Fluid Mech.* **248**, 297–313.

LEIBOVICH, S. 1970 Weakly non-linear waves in rotational fluids. *J. Fluid Mech.* **42**, 803–822.

LEIBOVICH, S. & RANDALL, J. D. 1972 Solitary waves in concentrated vortices. *J. Fluid Mech.* **51**, 625–635.

MAXWORTHY, T. 1972 The structure and stability of vortex rings. *J. Fluid Mech.* **51**, 15–32.

MAXWORTHY, T. 1974 Turbulent vortex rings. *J. Fluid Mech.* **64**, 227–239.

MOFFATT, H. K. & MOORE, D. W. 1978 The response of Hill's spherical vortex to a small axisymmetric disturbance. *J. Fluid Mech.* **87**, 749–760.

ORLANDI, P. 1990 Vortex dipole rebound from a wall. *Phys. Fluids* A 2, 1429–1436.

ORLANDI, P. & JIMÉNEZ, J. 1991 A model for bursting of near wall vortical structures in boundary layers. In *8th Symp. on Turbulent Shear Flows, September 1991, Munich*, pp. 28.1.1–28.1.6.

PERRY, A. E. & FAIRLIE, B. D. 1975 A study of turbulent boundary layer separation and reattachment. *J. Fluid Mech.* **69**, 657–672.

PIERREHUMBERT, R. T. 1980 A family of steady, translating vortex pairs with distributed vorticity. *J. Fluid Mech.* **99**, 129–144.

POZRIKIDIS, C. 1986 The non-linear instability of Hill's vortex. *J. Fluid Mech.* **168**, 337–367.

PULLIN, D. I. 1981 The nonlinear behaviour of a constant vorticity layer at a wall. *J. Fluid Mech.* **108**, 401–421.

PULLIN, D. I. & GRIMSHAW, R. H. J. 1983 Interfacial progressive gravity waves in a two-layer shear flow. *Phys. Fluids* **26**, 1731–1739.

PULLIN, D. I. & GRIMSHAW, R. H. J. 1988 Finite-amplitude solitary waves at the interface between two homogeneous fluids. *Phys. Fluids* **31**, 3550–3559.

RAYLEIGH, LORD 1887 On the stability or instability of certain fluid motions, II. In *Scientific Papers*, vol. 3. Cambridge University Press, pp. 17–23.

SAFFMAN, P. G. 1993 *Vortex Dynamics*, secs. 9.6 and 14.2. Cambridge University Press.

SAFFMAN, P. G. & SZETO, R. 1980 Equilibrium shapes of a pair of equal uniform vortices. *Phys. Fluids* **23**, 2339–2342.

SAFFMAN, P. G. & TANVEER, S. 1982 The touching pair of equal and opposite uniform vortices. *Phys. Fluids* **25**, 1929–1930.

SENDSTAD, O. 1992 Mechanics of three dimensional boundary layers. PhD thesis, Stanford University.

SHARIFF, K. & LEONARD, A. 1992 Vortex rings. *Ann. Rev. Fluid Mech.* **24**, 235–279.

SHARIFF, K., LEONARD, A. & FERZIGER, J. H. 1989 Dynamics of a class of vortex rings. *NASA TM* 102257.

STERN, M. E. & PRATT, L. J. 1985 Dynamics of vorticity fronts. *J. Fluid Mech.* **161**, 513–532.

TELES DA SILVA, A. F. & PEREGRINE, D. H. 1988 Steep, steady surface waves on water of finite depth with constant vorticity. *J. Fluid Mech.* **195**, 281–302.

TURFUS, C. 1993 Prandtl–Batchelor flows past a flat plate at normal incidence in a channel – inviscid analysis. *J. Fluid Mech.* **249**, 59–72.

WU, H. M., OVERMAN, E. A. & ZABUSKI, N. J. 1984 Steady-state solutions of the Euler equations in two dimensions: Rotating and translating V-states with limiting cases. I. Numerical algorithms and results. *J. Comput. Phys.* **53**, 42–71.